



Synthesis of ZnO nanoparticles using peels of *Passiflora foetida* and study of its activity as an efficient catalyst for the degradation of hazardous organic dye

Mujahid Khan¹ · Pundlik Ware¹ · Navinchandra Shimpi¹Received: 25 November 2020 / Accepted: 24 February 2021 / Published online: 6 April 2021
© The Author(s) 2021 **OPEN**

Abstract

Creating a sustainable and effective approach to handling organic contaminants from industrial waste is an ongoing problem. In the present study, ZnO nanoparticles (ZnO NPs) were synthesized under a controlled ultrasound cavitation technique using the extract of *Passiflora foetida* fruit peels, which act as a reducing (i.e., reduction of metal salt) and stabilizing agent. The formation of monodispersed and hexagonal morphology (average size approximately 58 nm with BET surface area 30.83m²/g). The synthesized ZnO NPs were characterized by a various technique such as UV–visible spectroscopy, X-ray diffraction (XRD), Fourier-transform infrared (FTIR), Scanning electron microscopy (SEM), energy-dispersive X-ray spectroscopy (EDX), Transmission electron microscopy (TEM), Thermogravimetric analysis (TGA) and Dynamic light scattering (DLS). Further, the XRD pattern confirmed the hexagonal wurtzite structure of synthesized ZnONPs. The ZnO NPs exhibit excellent degradation efficiency towards organic pollutant dyes, i.e., Methylene blue (MB) (93.25% removal) and Rhodamine B (91.06% removal) in 70 min, under natural sunlight with apparent rate constant 0.0337 min⁻¹ ($R^2=0.9749$) and 0.0347 min⁻¹ ($R^2=0.9026$) respectively. Zeta potential study shows the presence of a negative charge on the surface of ZnO NPs. The use of green synthesized ZnO NPs is a good choice for wastewater treatment, given their high reusability and photocatalytic efficiency, along with adaptability to green synthesis.

Keywords Dye degradation · *Passiflora foetida* LE · Ultrasound cavitation · Methylene Blue (MB) · Rhodamine B (Rh-B)

1 Introduction

Urbanization and rapid industrialization have proven to be a blessing to human society as well as a bane. A severe adverse impact on the water resources and the disposal of a large quantity of toxic waste in water systems is now a challenging wastewater management [1–4]. In consumer goods, including paints, printing inks, paper, pulp, and plastics, various dyes have been used for many years. Some organic dyes are widely used and released in water, such as in textiles and other industries [5–9]. Toxic chemicals such as insecticides and organic dyes may be contained in industrial wastewater. Colored organic dye

influences aquatic bodies because it inhibits sun rays and reduces the concentration of dissolved oxygen. This causes essential health and environmental issues in the marine environment. To accomplish a toxic-free green environment and promote the survival of living things, removing these industrial dye pollutants from wastewater gained massive attention among researchers. Several methods, such as adsorption, biological treatment, and heterogeneous photocatalysts, have been used for dye removal from wastewater [10, 11].

Nanoparticles tend to absorb the dye effectively because of their high surface-to-volume ratio, and the selected compound can be altered to improve their

✉ Navinchandra Shimpi, navin_shimpi@rediffmail.com | ¹Material Science Laboratory, Department of Chemistry, University of Mumbai, Santacruz (E), Mumbai 400 098, Maharashtra, India.



chemical affinity again [12, 13]. The multi-nanostructure photocatalyst ZnO [14, 15], Fe₂O₃ [16], TiO₂ [17], WO₃ [18] etc. has been an excellent material for the removal of organic micropollutants by water photodegradation, using various methods to resolve these problems.

One of the most efficient strategies is semiconductor-based photocatalyst. The primary subject of research is the photocatalyst process and, therefore, the production of such material. Much research effort has been directed towards the development of effective photocatalysts [19–21]. Photodegradation of organic dyes using semiconducting metal oxide nanoparticles is an efficient method for removing these dyes from the effluent. Even though TiO₂ has been mainly used for eco-friendly use as a metal oxide photocatalyst, ZnO has been suggested as a low-cost photocatalyst for the degradation of organic molecules in an aqueous solution [22–24]. All the previous studies are shown in Table 1.

ZnO semiconductor with direct bandgap ($E_g = 3.37\text{eV}$) is a highly explored n-type semiconductor owing to their high electron–hole binding energy (60 meV) [25], high thermo-mechanical stability, and useful piezoelectric and optoelectric devices. The use of ZnO nanomaterials in photocatalysis has gained a lot of interest compared to commonly used TiO₂ nanomaterials due to their exceptional catalytic activity and quantum performance [26–29]. However, ZnO NPs can be synthesized by physicochemical methods efficiently. These production methods are expensive and produce harmful chemical products during synthesis.

As an additional requirement to ZnO NPs, green synthesis of nanoparticles can be an environmentally friendly and fast approach to treating wastewater effluent from textile industries. To prepare ZnO NPs, comprehensive methods of synthetic routes are recorded. However, the researchers gained considerable attention from the green chemical method, and this method prohibits the use of organic solvents and surfactants. Interestingly, the synthesis of ZnO NPs mediated by plant extract exhibits specified crystal structure and successful dye degradation [30, 31]. Green technologies for the preparation of ZnO NPs will be an alternative that is superior to current methods. For example, due to their benignity and flexible versatility in chemical structure, the phytoconstituent in a plant extract may simultaneously serve as stabilizing agent/reducing agents when preparing nanomaterials. Here, we used a greener method to synthesize ZnO nanoparticles using *Passiflora foetida*, commonly referred to as the extract of passion fruit plants, as a potential bio-nanocatalyst. It's an exotic, fast-growing perennial tree. The *Passiflora* genus belongs to the Passifloraceae family, which includes passion fruit [32]. They are rich sources of bioactive compounds and thus serve as an essential raw material for the manufacture of drugs and have become a priority for the hunt for new drugs. Plants are essential, remarkable, and common sources for curing various diseases in the form of medicines. Plant leaves are used as a folk medicine for stress, anti-anxiety, and insomnia therapy. Its properties include sedative, antiproliferative, antibacterial, anti-anxiety, anti-spasmodic, leishmanicidal, emetic, wound dressing, and the anti-ulcer plant [33–35]. Alkaloids, phenols, glycosides,

Table 1 Previous work done in the literature

S. no	Catalyst	Catalyst mass	Dye	Light and intensity	Irradiation time (min)	Degradation efficiency (%)	Ref.
1	NCQDs/TiO ₂	1000 mg/mL	MB	LED panel (42 W)	420	86.9	[62]
2	TiO ₂ /C-dots	1000 mg/mL	MB	Tugstan halogen lamp	240	89	[63]
3	CQD/ α -Fe ₂ O ₃	500 mg/mL	MB	Halogen spotlight (400 W)	90	87.7	[64]
4	ZnO/CQDs	750 mg/mL	RhB	Visible fiber lamp (0.5 W cm ⁻²)	105	94	[65]
5	C-dots/WO ₃	300 mg/mL	RhB	Xe lamp (300 W)	120	94.4	[66]
6	ZnO	1 cm ² /10 mL	MB	8 W mercury lamp	120	45	[67]
7	ZnO	1 cm ² /10 mL	RhB	8 W mercury lamp	120	34	[67]
8	2% Fe-ZnO	10 mg	MB	150 W mercury lamp	180	92	[68]
9	Cu ₂ O/ZnWO ₄	100 mg	MB	300 W Xe lamp	90	90	[69]
10	RGO-Bi ₂ O ₃	10 mg	MB	500 W tungsten lamp	240	98	[70]
11	ZnO	0.01 g/50 ml	RhB	Solar	360	100	[71]
12	TiO ₂	40 mg/40 ml	RhB	Visible lamp	300	62.2	[72]
13	ZnTiO ₃	0.03 g/30 ml	RhB	Solar	180	49.5	[73]
14	ZnTiO ₃ @S	0.03 g/30 ml	RhB	Solar	180	94.74	[73]
15	ZnO NPs	1 mg/ml	MB	Sunlight	70	93.25	Present work
16	ZnO NPs	1 mg/ml	RhB	Sunlight	70	91.06	Present work

passifloricins, flavonoids, cyanogenic compounds, polypeptides, and alpha pyrones are the constituents of *P. foetida*. *P. foetida* was used for the synthesis of various nanoparticles such as Ag [36], Cu [37], and Iron oxide [38], etc.

In this study, we prepared ZnO NPs using the ultrasound-assisted green synthesis method. Further, its photocatalytic activity was studied using MB and RhB dye under solar light irradiation. The high molecular masses and low diffusion rates make them challenging to degrade, the industrial dye MB and RhB were selected of these photocatalytic degradation study dyes. This is the first research to the best of our knowledge towards an ultrasonic approach to the synthesis of monodisperse ZnO NPs using Stinking passion fruit peels extract and its application for the degradation of MB Rhodamine B dye in solar irradiation. In addition to outstanding dye degradation performance, the as-synthesized ZnO NPs are known for easy recovery and reusability. This study demonstrates that ultrasound-assisted synthesis of ZnO NPs effective for dye degradation without artificial light sources. This study provides a new perspective into the green and cost-effective photocatalyst sector to relieve the harmful dyes high degradation efficiency from industrially contaminated water without harming or generating another environmental hazard.

1.1 Experimental work

1.1.1 Materials

MB (Methylene Blue; $C_{16}H_{18}ClN_3S$ -82%) and Rh-B (Rhodamine B; $C_{28}H_{31}ClN_2O_3$ -80%) were procured Sigma Aldrich, India. $Zn(NO_3)_2 \cdot 6H_2O$ (99%) and NaOH (98.5%) were obtained from fine chemicals (Mumbai, India). The chromic acid was used to clean all mandatory glassware and with deionized water. Fresh fruit was collected from Mumbai University garden, Kalina Campus, Mumbai.

1.1.2 Preparation of *Passiflora foetida* fruit peels extract

The contaminants from the ripened *Passiflora foetida* fruits surface were removed by washing with tap water and distilled water and dried under ambient conditions. The dried peels were grounded into a fine powder. Further, peels powder (25 g) was added into 200 mL water in a 250 mL beaker and subjected to stirring for 30 min at 70 °C. The color of distilled water turns to pale yellow. The obtained solution passed through Whatman filter paper number 42 and centrifuged at 7000 rpm and synthesized nanomaterials.

1.1.3 Synthesis of ZnO nanoparticles using Ultrasound cavitation technique

In $Zn(NO_3)_2 \cdot 6H_2O$ (100 mM) solution, 125 mL of peels extract was added under controlled ultrasound at 80% frequency with on and off time 4/2 s and sonicated next 30 min. After the complete mixing of salt solution and peel extract, the addition of 100 mL NaOH (200 mM) was done dropwise after the addition solution was kept under ultrasonic probe sonicator (SJIA-250 W, 220 V, 20 kHz, 4-s loud screeching noise) for the next 90 min. The solution color turns from pale yellow to whitish-yellow during the reaction, indicating salt reduction into $Zn(OH)_2$. The obtained precipitate was centrifuged at 7000 rpm for 10 min. Then precipitated was dispersed in deionized ethanol/water and centrifuged (7000 rpm, 10 min). To get a high purity of ZnO NPs, the precipitate was repeatedly centrifuged and better-eliminated impurities. Finally, the residue was calcinated at 400 °C for one h. Figure 1 shows the path followed for the synthesis of ZnO.

1.1.4 Characterization

Centrifugation was carried out at 7000 rpm using a Remi R24 machine. Shimadzu UV 2450 was used for UV–vis study, pro-SHIMADZU RF 5300PL spectrophotometer was used to record the Photoluminescence (PL) spectrum at room temperature quartz cuvette of 1 cm path. Zetasizer Nano ZS90 was used for particle size distribution and Zeta potential measurements by Dynamic light scattering (DLS) measurements, with a red laser (633 nm) and an avalanche photodiode detector (quantum efficiency > 50%, Malvern Instruments Ltd., UK). SHIMADZU 7000S was determined X-ray powder diffraction (XRD) within commission voltage 40 kV, current 30 mA, scan speed 10 min^{-1} , monochromatic $CuK\alpha$ radiation ($\lambda = 1.5406 \text{ \AA}$) in the 2θ range of 25–80 °C. The average nanocrystalline size is calculated by the Debye–Scherrer Eq. (1).

$$\text{Average crystalline size} = (0.9 \times \lambda) / (d \cos \theta) \quad (1)$$

where $\lambda = 1.54060 \text{ \AA}$ (for $CuK\alpha_1$), d is the full width at half maximum intensity of the peak (in Rad) and $\theta = 2\theta/2$. To decipher the vibrational in a sequence of functional moieties present in peels and ZnO, PERKIN ELMER FRONTIER 91,579 was used for Fourier-transform infrared (FT-IR) in the sequence $4000\text{--}400 \text{ cm}^{-1}$ at a resolution of 4 cm^{-1} . JEOL JSM-7600F determine FEG-SEM with group EDX from IIT, Mumbai.

Further, morphology study and particle size were analyzed using FESEM (Hitachi S-4800, Japan). Elemental

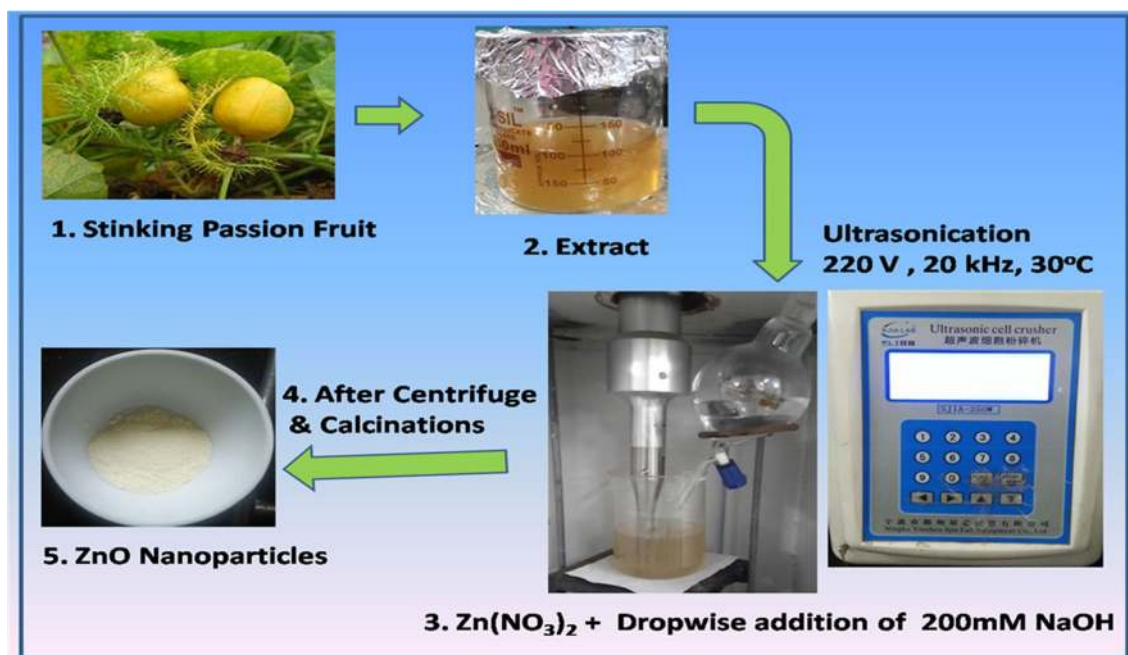


Fig. 1 Schematic representation of the synthesis of ZnO NPs

analysis was done using Energy-dispersive atomic X-ray analysis (EDAX). Transmission electron microscopy (TEM) (A JEOL JEM 2100) instrument was used for particle size measurement. Thermogravimetric analysis was done from 30 to 1000 °C at a heating rate of 5 °C/min under a nitrogen atmosphere using the STAR system METTLER TOLEDO.

Further, the surface area of nanoparticles was measured by Brunauer–Emmett–Teller (BET), and Barret-Joyner-Halendra (BJH) analysis was done for pore size distribution studies using N₂ adsorption–desorption isotherm (AutosorbIQ station2).

1.1.5 Photocatalytic activity

Using nanoparticles as a catalyst (1 mg/mL) into a 100 mL solution of methylene blue (10 ppm) and Rhodamine-B dye molecule (10 ppm), photocatalytic degradation of MB and Rh-B was performed under sunlight. Synthesized catalysts that were subjected to direct sunlight, the degradation behavior were investigated under solar light irradiation. At 36–40 °C, the whole experiment was conducted. 1 mL of suspension was collected and centrifuged after a corresponding time interval (10 min), and its absorption was measured using UV–Vis spectroscopy within the 200–800 nm wavelength range. The photocatalyst efficiency in organic dye degradation was measured using the following Eq. (2)

$$\% \text{ of degradation} = \frac{(C_0 - C_t)100}{C_0} \quad (2)$$

where C_0 is the initial absorbance and C_t is the absorbance of the Rh-B and MB dye after reaction time (t) in min.

With the help of pseudo-first-order kinetic models from Eq. (3), it is possible to determine the quantitative kinetics of the increased photocatalytic motion and degradation in MB and Rh-B concerning time.

$$\ln C_t = K_{1app} - t + \ln C_0 \quad (3)$$

K_{1app} is apparent rate steady for the pseudo-first-order kinetic model, C_0 is initial absorbance, and C_t is the absorbance at time t.

1.1.6 Chemical oxygen demand (COD)

The reported standard procedure carried COD measurement; the organic contaminants in the MB and Rh-B dye samples were analyzed by potassium dichromate titration [7, 39]. The dye sample was refluxed in the presence of HgSO₄ and Ag₂SO₄ in H₂SO₄ medium, and it was further refluxed with a known volume of standard potassium dichromate solution. The solution was titrated against standard ferrous ammonium sulfate (FAS) to estimate the amount of potassium dichromate, using the ferroin indicator. A blank experiment was also performed with distilled

water instead of the dye sample. The following formula was used for the COD calculation:

$$\text{COD} = (\text{Blank titer value} - \text{Dye sample titer value}) \times \text{Normality of FAS} \times 8 \times 1000.$$

the volume of the sample taken.

2 Results and discussion

2.1 Optical properties

The conversion of $\text{Zn}(\text{NO}_3)_2$ to ZnO was confirmed by the UV-vis spectra shown in Fig. 2. During ZnO synthesis, the

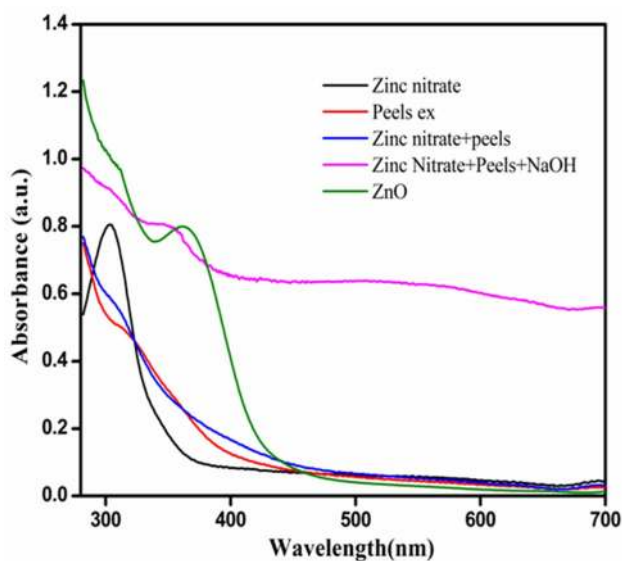


Fig. 2 UV-vis absorption spectra of ZnO NPs

maximum wavelength of 300 nm of $\text{Zn}(\text{NO}_3)_2$ shifts from 340 to 370 nm. The yellowish color of stinking passion fruit peels extracts ends with whitish color shows the complete formation of $\text{Zn}(\text{OH})_2$. The instant white-yellowish color appearance in peels extract shows reaction go towards the formation of ZnO NPs. This is due to restricted Surface Plasmon Resonance (SPR) due to the combined oscillation of free transference electrons [26].

Figure 2 shows that the SPR fascination of ZnO NPs gave at $\lambda_{\text{max}} = 524$ nm with the absorbance of 0.809 a.u.

Figure 3 shows UV-Visible spectroscopy study of ZnO NPs carried out using diffuse reflectance spectroscopy (DRS) mode. Strong absorption was observed at a wavelength ranging from 200 to 380 nm. ZnO is a direct band-gap semiconductor with a bandgap of 3.37 eV. Thus, tauc's equation is used to calculate the bandgap [40].

$$(\alpha h\nu) = A(h\nu - E_g)^n$$

here, n is $1/2$ for direct transition semiconductor A is constant, and α is adsorption coefficient. The absorption plot was converted to tauc's plot $[(\alpha h\nu)^2 \text{ vs. } h\nu]$ using absorption onset. The UV-vis spectrum of ZnO nanoparticles shows the 357 nm could be attributed to electron transfer from the valence band to the conductive band, related to ZnO intrinsic bandgap absorption ($\text{O}2p\text{-zn}3d$) [41]. The bandgap for the ZnO nanoparticles was found to be a 3.16 eV bandgap.

Figure 4 shows photoluminescent (PL) spectrum is related to the recombination of photoinduced electrons and holes, free excitons, and self-induced excitons. This PL emission spectrum is most important in investigating the efficacy of charge carrier trapping and its transport mechanism [42–44]. The biogenic photo luminescent view shown in Fig. 4 at temperature PL of synthesized ZnO NPs shows an emission peak at 524 nm with intensity

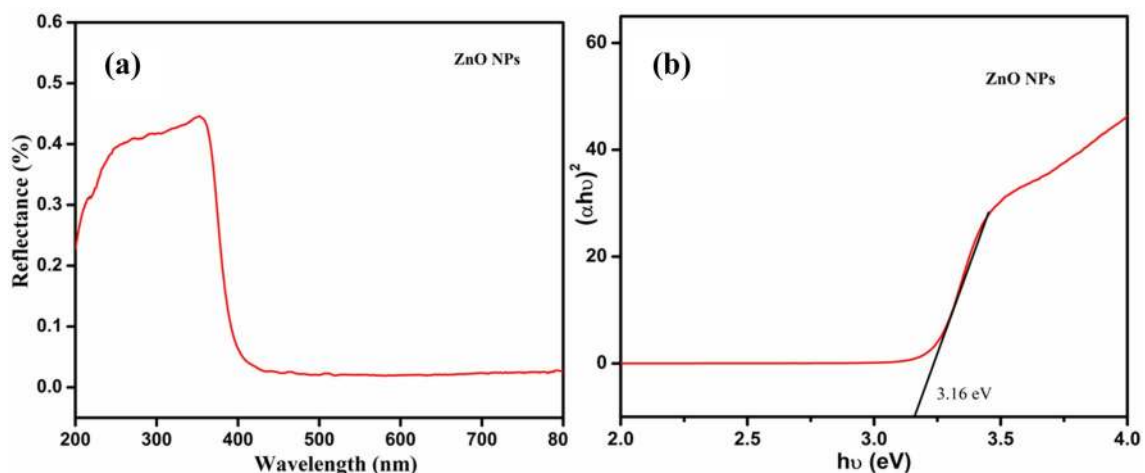


Fig. 3 a DRS spectra of ZnONPs b Tauc's plot

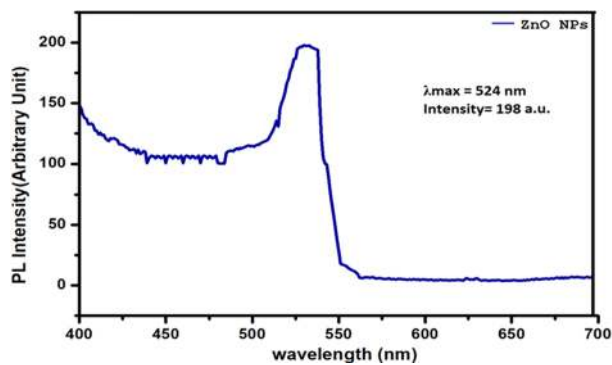


Fig. 4 Photoluminescence spectra of ZnO NPs at room temperature

198.028 a.u. was sensibly using bandgap excitation (368 nm). The PL emission rate is directly proportional to the photo-excited load carriers recombination probability. Higher PL Strength points to advanced e^-/h^+ pair recombination and guides to the lower photocatalytic activity [45, 46]. In comparison, lower PL intensity indicates lower e^-/h^+ pair recombination, illuminating high photoinduced charge carrier partition competence and higher photocatalytic operation [47, 48]. Lesser recombination rate and higher photocatalytic activity due to the low intensity of ZnO NPs indicate a less extrinsic flaw in the crystalline arrangement.

3 Structural properties

Figure 5 shows the XRD spectra of stinking passion fruit peel powder, which showed a hump, which indicates the amorphous nature of stinking passion fruit powder. Further, XRD spectra of ZnO nanoparticles shows the diffraction peak at $2\theta = 31.74, 34.38, 36.18, 47.50, 56.72, 62.86$ and 67.98° correspond to (100), (101), (102), (110), (103) and (112) lattice planes respectively ZnONPs (JCPDS card: 79-2205) embedded. The average crystalline size was specified using well known Scherrer formula [49, 50]. The average crystalline size was found to be obtained 23.8 nm from the XRD pattern. The peaks in Fig. 5b are characteristic of the ZnO polycrystalline wurtzite structure of the hexagonal crystal system. The existence of ZnO is confirmed by X-ray diffraction peaks, FTIR, and UV-Vis spectra. Further, FEG-SEM, TEM, and EDX will support the results.

4 FTIR analysis

The FTIR spectrum clears the potential organic support complex to help stabilize and cap Zinc oxide nanoparticles. Stinking passion fruit peels take out derived ZnO,

Fourier transform infrared (FTIR) spectra of the samples were evidence in the series of $400\text{--}4000\text{ cm}^{-1}$. The FTIR spectra of Stinking passion fruit peels extract Fig. 6a shows the peak at $3486, 3209, 2980\text{ cm}^{-1}$ associated with the intermolecular hydrogen-bonded -OH group phenol. The peak at 3486 cm^{-1} of Stinking passion fruit peels removes completely after ZnO formation. Furthermore, C=O amide band stretching at 1650 cm^{-1} , which participated in stabilization by developing amide group protein encapsulation and protected next to aggregation. The OH stretching band at 1051 cm^{-1} bending vibrations attributed to water molecules present in the catalyst. Further, Fig. 6b demonstrate the FTIR spectrum of ZnO NPs. For this sample, the band at $460, 1648, \text{ and } 3417\text{ cm}^{-1}$ is attributed to Zn-O, O-H bending and stretching vibration of O-H groups [51]. The peak below 500 cm^{-1} indicates formation, which is mainly expected due to flavonoid (polyphenol) compounds and stabilized by protein molecule. Further, a peak of 529 cm^{-1} appeared due to S-S disulfide protein bonding, as shown in Table 2. Peak associated with OH is absent in the FTIR spectra of ZnO nanoparticles due to nanoparticle calcination. The observed peak at 1645 and 1323 cm^{-1} attributed to asymmetric and symmetric stretching carboxylate.

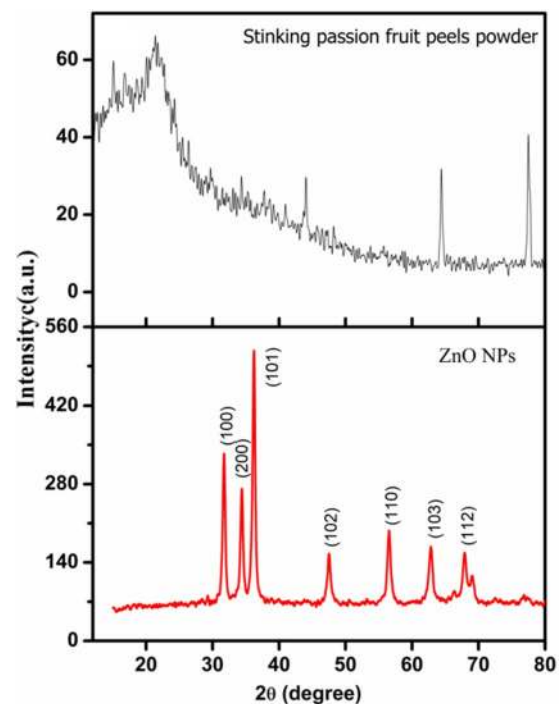


Fig. 5 XRD spectra of Stinking passion fruit peels powder and ZnO NPs

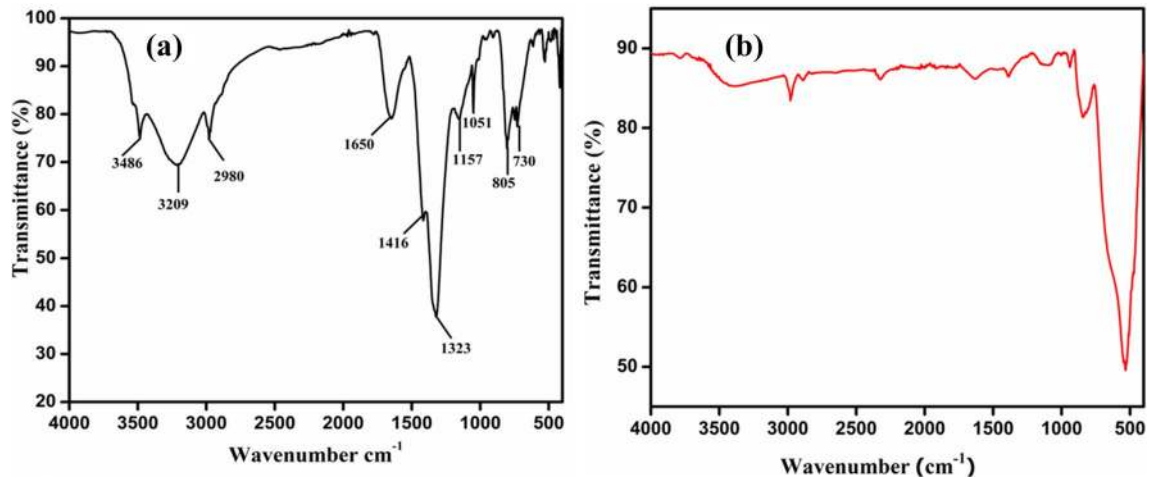


Fig. 6 FTIR spectra **a** Stinking passion fruit peels extract **b** ZnO NPs

Table 2 FTIR of Stinking passion fruit peel and ZnO nanoparticles

Sample	Characteristic wavenumbers (cm ⁻¹) with a functional group
Stinking passion fruit peels	3486 cm ⁻¹ (N-H), 3209 cm ⁻¹ ((nO-H), 2980 cm ⁻¹ (nC-H assymetric), 1650 cm ⁻¹ (nC=O amide), 1416 cm ⁻¹ (nC=C), 1157 cm ⁻¹ (C-O-C), 1051 cm ⁻¹ (nO-H bending vibrations), 805–730 cm ⁻¹ (C=C tri substituted alkene), 529 cm ⁻¹ (nS-S cysteine protein)
ZnO	1645 cm ⁻¹ , 1323 cm ⁻¹ (asymmetric and symmetric of stretching carbonxylate)

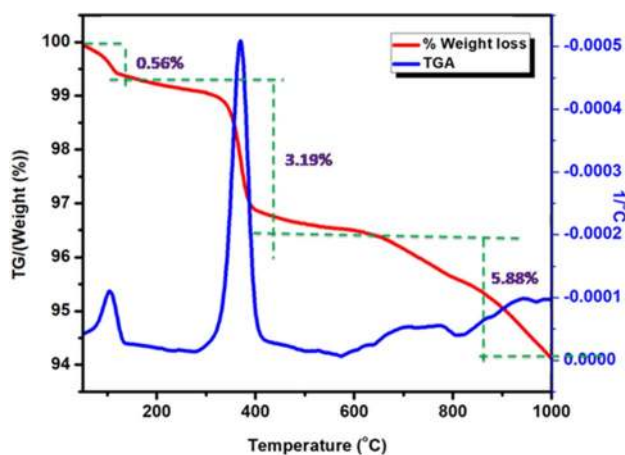


Fig. 7 Thermogravimetric analysis of ZnO

5 TGA study

ZnO NPs derived from stinking passion fruit peels 0.56%, 3.19%, and 5.88% were originate to be thermally stable. As indicated in Fig. 7, ZnO showed decomposition after 133 °C, while after 400 °C indicating improved thermal constancy. First step weight thrashing 3.19% of the

Table 3 Thermogravimetric analysis of Stinking passion fruit peels extract and derived ZnO NPs

Sample	Start T	End T	Weight loss%	Residual @T
ZnO	100 °C	133.8 °C	0.56	99.36%@133.8 °C
	133.8 °C	412 °C	3.19	96.67%@412 °C
	412 °C	1000 °C	5.88	94.11%@1000 °C

subsequent step weight loss 5.88% was experiential due to taking away organic and inorganic moieties from ZnO NPs (Table 3).

6 Measurements of zeta potential, DLS, and BET study

Figure 8 shows the Zeta potential of ZnO NPs. Further, the average particle size was calculate using DLS. The three measurements were conducted at 25 °C for repeatability. The DLS results are expressed by plotting total counts against apparent zeta potential. When ZnO NPs dispersed in water move from side to side in a liquid medium, frequently a thin, electric dipole coating adheres to its plane, i.e.,

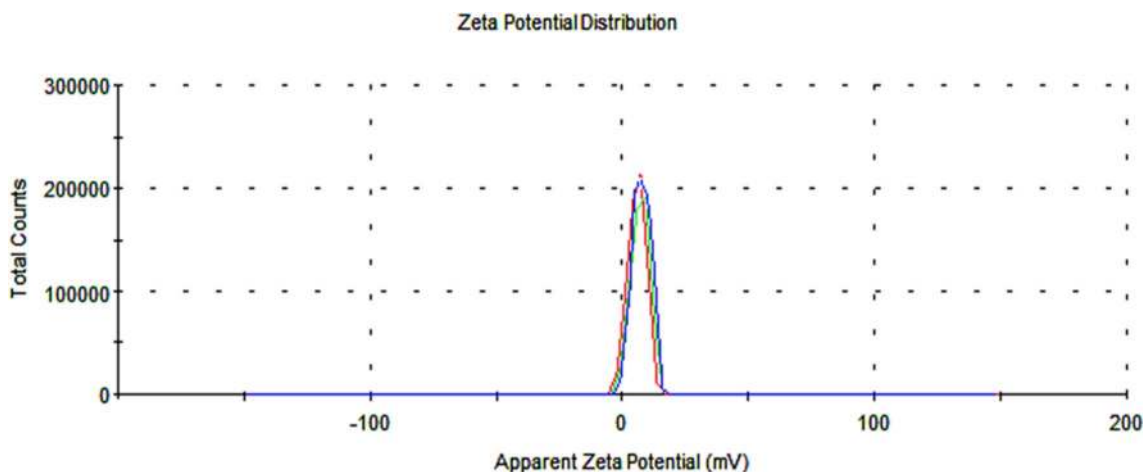


Fig. 8 Zeta potential analysis of zinc oxide NPs

Table 4 Zeta potential and dynamic light scattering measurements

T °C	Z-Avg (d nm)	Polydispersity index (PDI)	Zeta potential (mv)	Mobility (μmcm/Vs)	Conductance (mS/cm)
25	522	0.292	-23.4	-1.832	0.0197
25	534	0.231	-23.1	-1.802	0.0198
25	526	0.245	-22.5	-1.763	0.0198
Mean	527.33	0.256	-23.3	-1.799	0.01976

hydrodynamic particle diameter size was 360 nm (Table 4). The zeta potential of ZnO NPs shows stability in the aqueous solution. A zeta potential value of -23.3 mV (Fig. 8) indicates that the dispersed ZnO NPs were capped by negatively charged groups proving that they are stable. Moreover, in Fig. 8, the curves nature indicates ZnO distribution in water was uniform and homogeneous. The ionic mobility and conductance of hydrodynamic ZnO NPs were $-1.799 \mu\text{mcm/Vs}$, and 0.01976 mS/cm shows good stability in a liquid medium.

Besides, a BET analysis was used to investigate the surface structure of synthesized ZnO NPs (Fig. 9). The BET specific surface area was determined by performing nitrogen adsorption–desorption measurements at 77 K, and the BJH method was used to assess the distribution of nanoparticles pore size. The result for BET in Fig. 9 suggests that ZnO has a porous structure, as shown by the isotherm of N₂ adsorption and desorption. Besides that, based on the IUPAC classification, the observed hysteresis loop is related to type H4. For ZnO NPs, the surface area was $30.83 \text{ m}^2/\text{g}$, and the distribution of pore volume and pore diameter was eased by the BJH method.

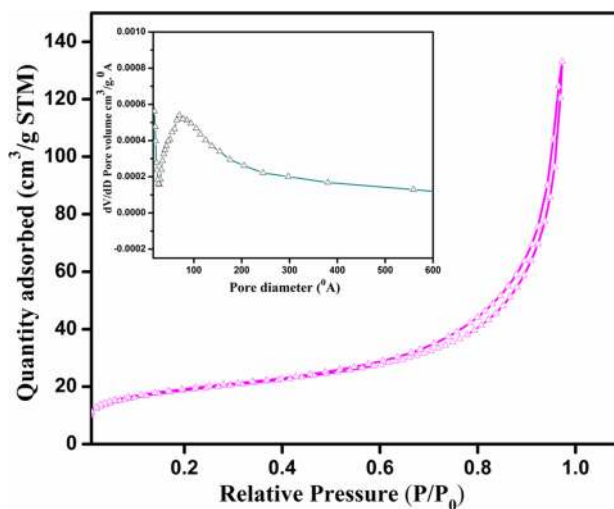


Fig. 9 BET of ZnO NPs

7 FESEM study

Figure 10 shows the FEG-SEM of ZnO NPs shows hexagonal morphology with a size of approximately 58 nm. EDX pattern of ZnO NPs shown in Fig. 10 give the existence of Zn and O elements. Copper (Cu) and Carbon (C) were appeared due to the outside layer during sample preparation. The EDX pattern indicates elevated cleanliness of as-synthesized ZnO NPs. FEG-SEM image of ZnO NPs showed virtually spherical morphology with standard particles of $\sim 58 \text{ nm}$ size (Fig. 10a and b). A difference in morphology depends on reactants attention, dipolar, intrinsic crystal concentration, taster processing, hydrophobic magnetism,

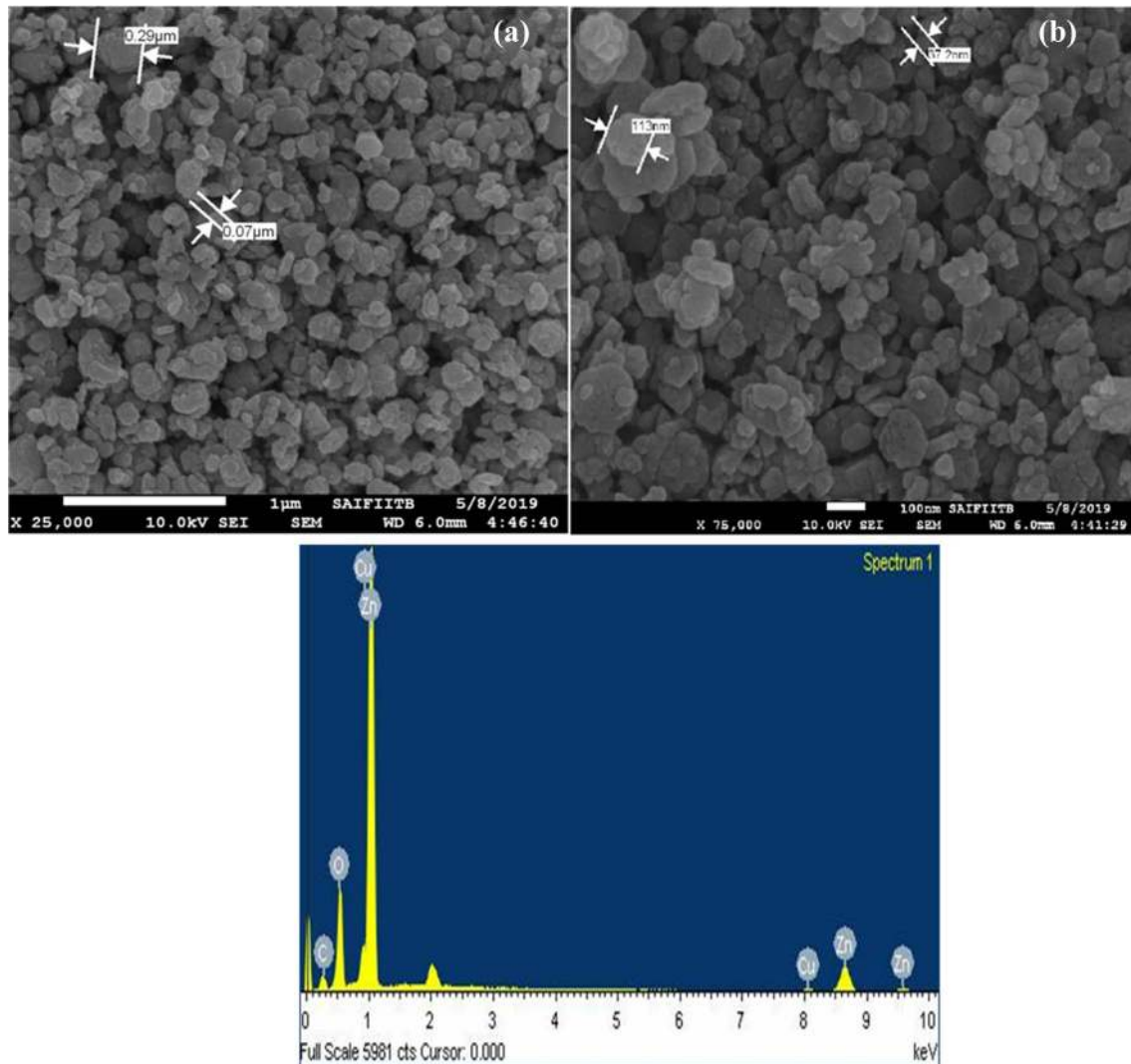


Fig. 10 FEG-SEM and EDAX of ZnO NPs

Vander Waal forces, and electrostatic fields. Moreover, kinetic and energetic aspects of synthesis also influence morphology [52, 53].

8 TEM study

Figure 11a-b shows the TEM images of synthesized ZnO nanoparticles; The TEM picture with SAED pattern has concentric circles dotted with bright spots. This shows the very crystalline existence of these NPs. and these concentric rings can be recognized to the diffraction from the {100}, {101}, {102}, {110}, {103} and {112} plane of the structure polycrystalline wurtzite structure of hexagonal crystal system. To get a cavernous approaching into morphology and exact microstructure inquiry, ZnO NPs were confirmed through TEM techniques. Interactions and embedding of

ZnO NPs are visible. The ZnO nanoparticles polycrystalline nature was promoted by the chosen region electron diffraction (SAED) blueprint under different magnification (Fig. 11c–d). Besides, TEM images (Fig. 11a–b) of ZnO were given to further proving the Hexagonal morphology, which in agreement with XRD results.

9 Catalytic performance

The synthesized ZnO NPs show the potential application in the degradation of methylene blue (MB) and rhodamine B (Rh-B) dyes. The photocatalytic activity of ZnO nanoparticles was investigated by analyzing MB and Rh-B dyes degradation behavior as a function of irradiation solar irradiation. The photocatalytic degradation of MB and Rh-B using ZnO nanoparticles was studied (Fig. 12e–f).

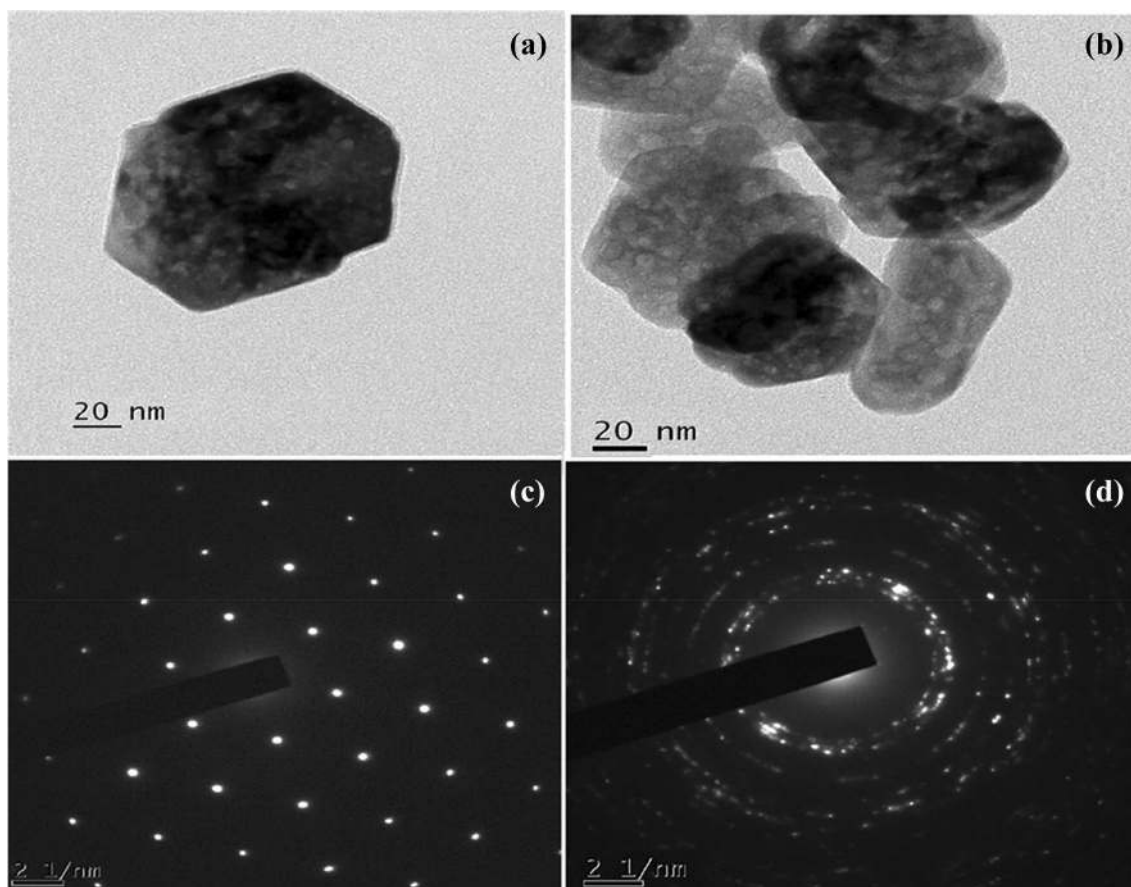


Fig. 11 TEM images of ZnO(**a** and **b**) and the corresponding SAED pattern (**c** and **d**)

The absorption of each dye for ZnO nanoparticles was recorded at every interval of 10 min using the UV-Vis spectroscopic technique upon exposure to light. Figure 12 a-b shows that blank experimental studies show that both the dyes do not degrade significantly without photocatalyst. The findings show that after 70 min of light irradiation, the blank dye degraded to 9.17% (MB) and 8.89% (RhB), which shows that the dye shows stability and does not undergo rapid degradation when exposed to light. Therefore, for effective dye degradation, a photocatalyst is required. Besides, the effect of the photocatalyst on dye degradation was studied under dark conditions [51, 54]. Figure 12c, d shows dye degradation under dark conditions. Following the addition of the photocatalyst, the dye solution was processed for 70 min under dark conditions. The photocatalyst surface has been shown to absorb approximately 25% MB and 19% Rh-B dye. Effective degradation due to

the photocatalytic effect of ZnO NPs has been observed after sunlight exposure.

The λ_{\max} for MB and Rh-B was found to be 663 nm and 554 nm, respectively. The presence of ZnO nanoparticle absorption maxima for MB decreased gradually and disappeared completely after 70 min and showed 93.25% MB dye degradation. Similarly, the degradation pattern observed for the Rh-B at 70 min using ZnO nanoparticles shows 91.06% degradation, as shown in Fig. 12e, f. Changes in peak absorption intensity indicate a change in MB and Rh-B chromophoric structure due to the ZnO nanoparticles effective photocatalytic activity. The photocatalytic efficiency was calculated using the following.

$$\text{Degradation}(\%) = 1 - \frac{C}{C_0}$$

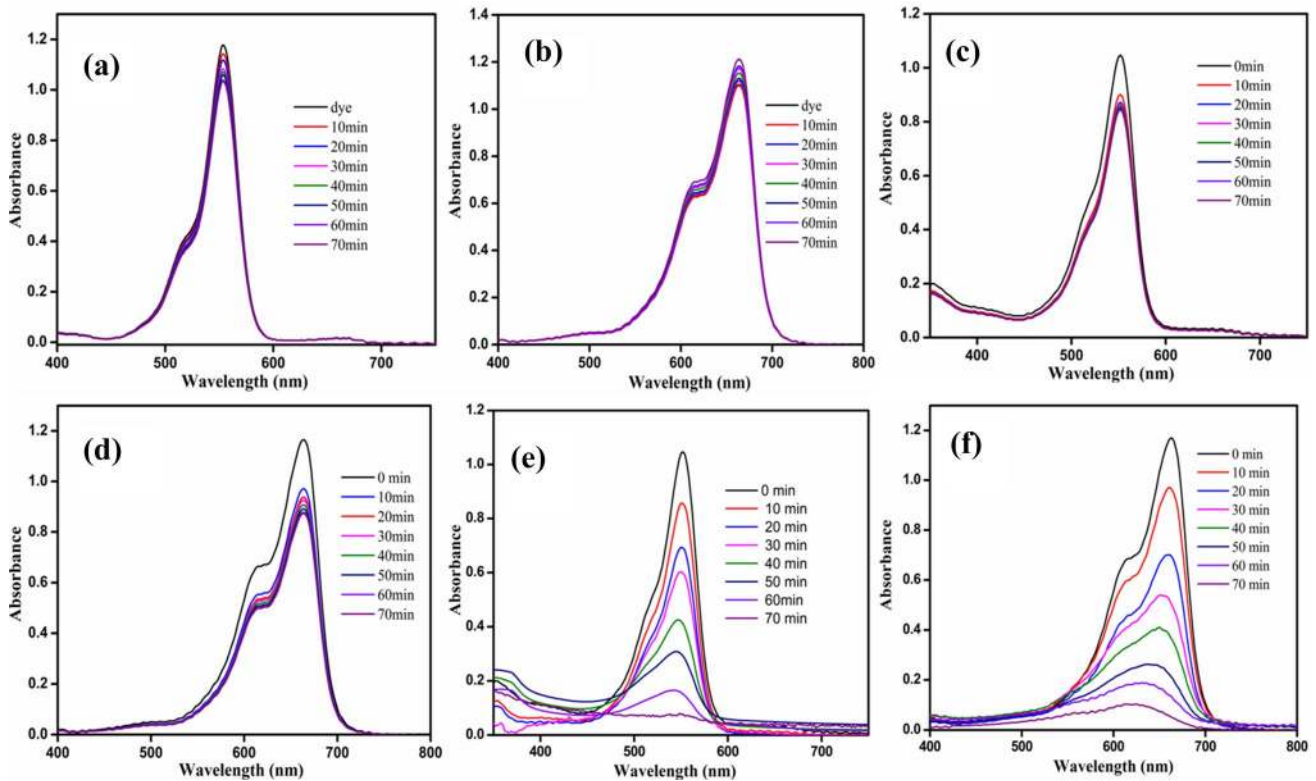


Fig. 12 Absorption study of (a, b) blank dye (c, d) dye absorption in dark and (e, f) degradation of MB and Rh-B

% degradation and kinetic treatment

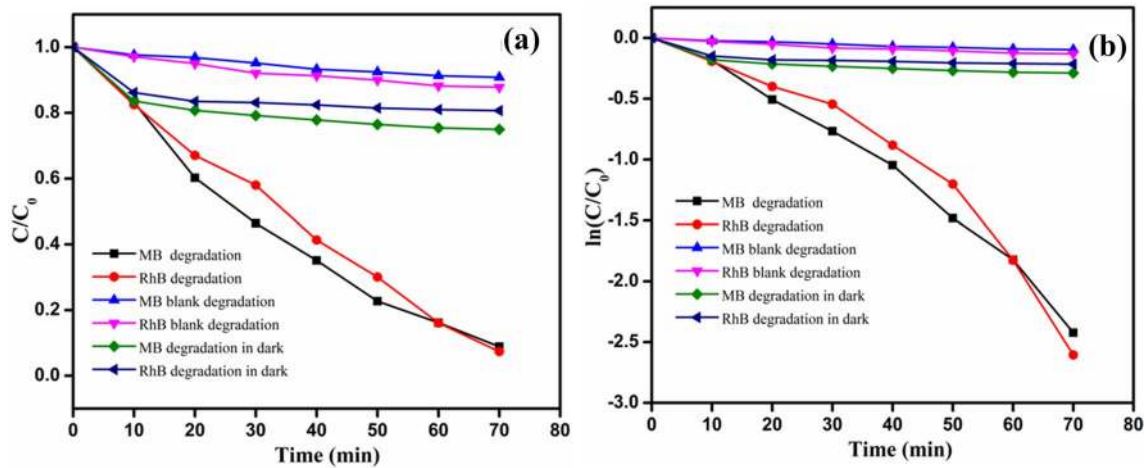


Fig. 13 Degradation kinetics of MB and Rh-B

10 % degradation and kinetic treatment

Experimentally acquire standards from the pseudo-first-order equation were fitted in the kinetic rate equation of C/C_0 versus time (min) and $\ln C/C_0$ versus T (min)

shown in Fig. 13a–b. The linearity in degradation pattern indicated that photodegradation of Rh-B and MB followed pseudo-first-order. The pseudo primary order, the apparent rate constants (K_{1app}) of ZnO for Rh-B and MB were established to be 0.0347 min^{-1} ($R^2 = 0.9026$)

and 0.0337 min^{-1} ($R^2 = 0.9749$) in that order. High values of rate stability indicate dye degradation successfully processed by ZnO NPs. The high photocatalytic activity of ZnO is due to the high surface area, which leads to maximum surface charge interaction with dye molecules. The MB and Rh-B dye (cationic) bound with negative charge surface of photocatalyst [55, 56]. The neutral pH of Rh-B ($\text{C}_{28}\text{H}_{31}\text{ClN}_2\text{O}_3 = \text{C}_{28}\text{H}_{31}\text{N}_2\text{O}_3^+ + \text{Cl}^-$) and MB ($\text{C}_{16}\text{H}_{18}\text{ClN}_3\text{S} = \text{C}_{16}\text{H}_{18}\text{N}_3\text{S}^+ + \text{Cl}^-$) both are positively charged get targeted by negatively charged hydrodynamic surface of ZnO NPs. Well-built adsorption of a substrate on the ZnO catalyst surface proceeds with a fast and high degradation rate. Rh-B and MB have the same $=\text{N}(\text{CH}_3)_2^+$ positively charged group. Their adsorption capacity over the ZnO surface is dissimilar due to the difference in size [57]. Due to ZnO lower PL intensity, sunlight shows photocatalytic activity (Fig. 13) and high separation of e^-/h^+ pair. Due to free electrons, H_2O and O_2 converted into free active particles like O_2^- , OH^\cdot and HO_2^\cdot . These free particles degrade dye into CO_2 , H_2O , and other molecules.

As a result, it was found that ZnO could competently accelerates photogenerated charge carriers and carry out faster photodegradation kinetics from pseudo-first-order revealed the apparent kinetic rates were 0.0347 min^{-1} ($R^2 = 0.9026$) and 0.0337 min^{-1} ($R^2 = 0.9749$) through Rh-B and MB degradation.

11 Effect of active oxidizing species on dye degradation and COD analysis

Depict the process of dye degradation mechanism by ZnO nanostructure upon irradiation of sunlight. Exposure of ZnO nanostructure to sunlight leads to an electron in the conduction band and holes in the valence band ($\cdot\text{OH}$) upon interaction with water. Further, these free radicals interact with the adsorbed organic dye molecules and degrade or mineralize them into non-toxic products. The effect of different oxidizing active species on MB and Rh-B degradation over ZnO nanoparticles is shown in Fig. 15a.

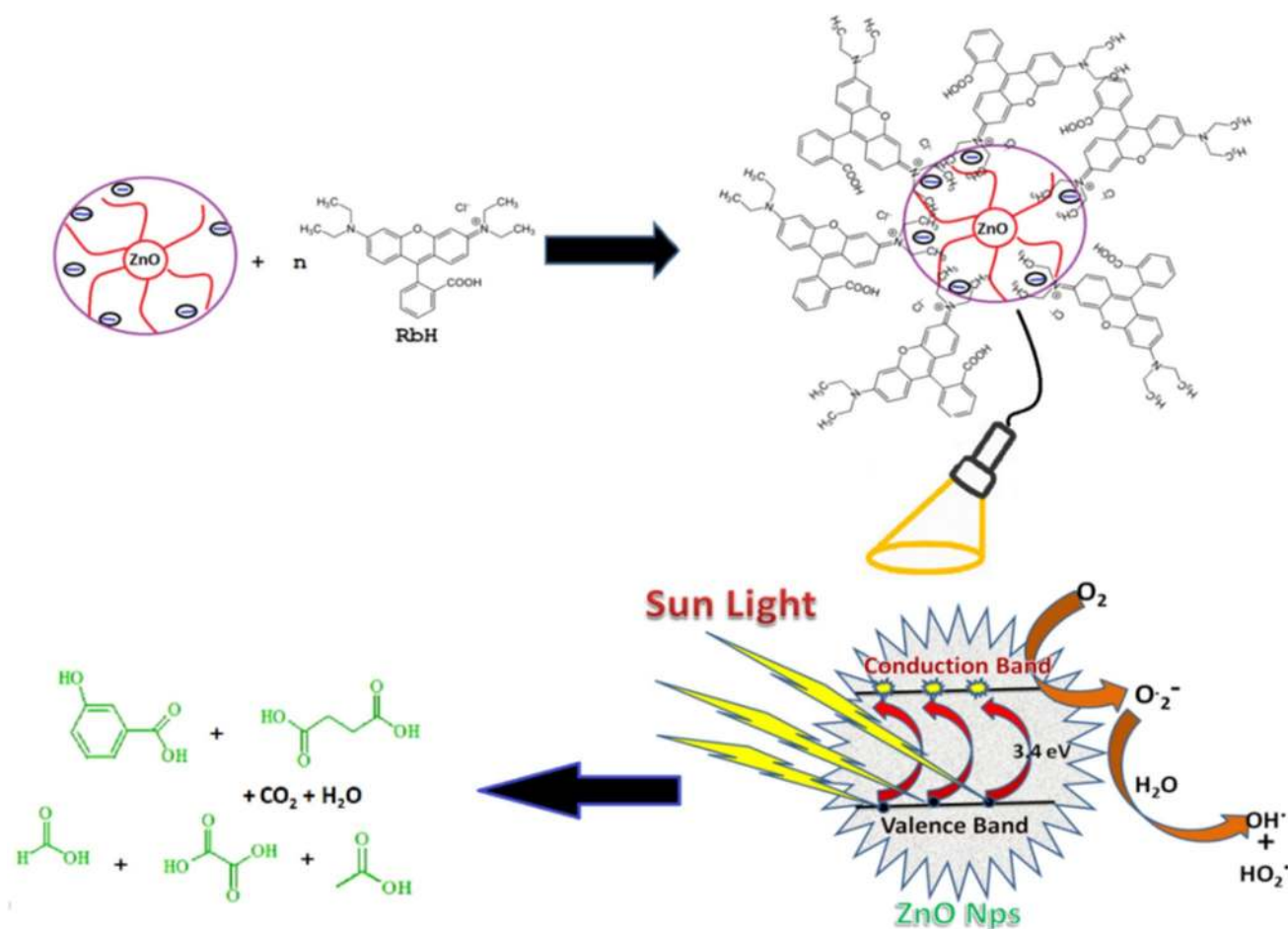


Fig. 14 Schematic mechanism for degradation of dyes

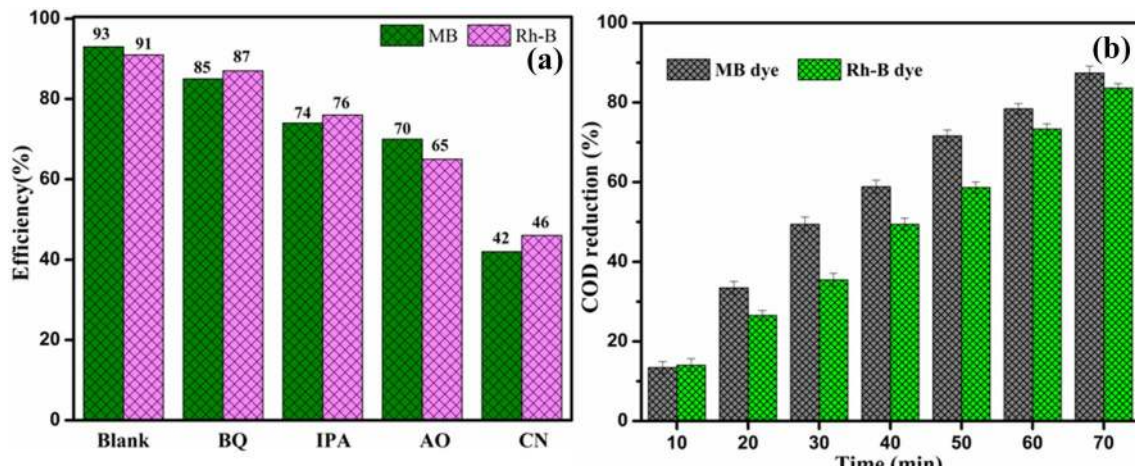


Fig. 15 a Scavenger study b COD analysis

The photocatalytic degradation reaction is carried out by introducing benzoquinone (BQ), isopropyl alcohol (IPA), ammonium oxalate (AO), and cupric nitrate (CN) were used as a quencher for photogenerated $\cdot\text{O}_2^-$, $\cdot\text{OH}$, h^+ and e^- [58, 59]. As shown in Fig. 14a, maximum photocatalytic degradation (93.25%) of MB and (91.6%) Rh-B dye was achieved without any scavenging intermediate.

The photocatalytic activity of prepared ZnO NPs was found to be decreased in the presence of scavengers. The addition of (Benzoquinone) BQ in the photocatalytic system was found to result in a slight reduction in the efficiency of ZnO NPs. Photocatalytic efficiency decreased by only 3.5% and 2.1% for ZnO NPs, respectively, compared to efficiencies without scavenger. This shows the negligible minor role of $\cdot\text{O}_2^-$ radicals towards the degradation of both dye. Addition of isopropyl alcohol (IPA, resulted in a 25.42 and 23.32% reduction in the photocatalytic efficiency for ZnO NPs. The photocatalytic efficiency of ZnO NPs decreased by 29.22% and 35% for MB and Rh-B dye upon addition of ammonium oxalate (AO). This shows that $\cdot\text{OH}$ and h^+ play a minor role in deciding the photocatalytic activity of the prepared ZnO NPs. The addition of cupric nitrate (CN) led to a significant reduction in the photocatalytic efficiency of ZnO NPs. The observed significant reduction of 58 and 54% in the photocatalytic efficiency of ZnO NPs. The addition of CN clearly shows that photogenerated e^- plays a significant role in the photocatalytic degradation of dyes. In other words, the relative dominance of ROS species in the photocatalytic processes can be estimated as $\text{e}^- > \text{h}^+ > \cdot\text{OH} > \cdot\text{O}_2^-$.

Also, the chemical oxygen demand (COD) was measured in Fig. 15b. The mineralization of MB and Rh-B dye solution was evaluated by COD examination. COD

was taken after each time interval after photocatalyst loading. The dichromate titration determined a percent reduction in COD. The highest percentage of COD reduction was reported at 87.41 and 83.62% for MB and Rh-B dyes. Due to the formation of certain intermediate (uncloured) mounts that can interfere in the degradation process, complete dye mineralization does not occur [60].

12 Reusability and photostability of ZnO nanoparticles

Catalyst reusability indicates that a possible catalyst is reusable many times, possessing about the same efficiency percentage. Therefore, investigating the reusability of synthesized catalysts is essential [61, 62]. The evaluation of synthesized ZnO for MB and Rh-B dye photodegradation has been studied through five consecutive batch processes. Figure 15a showed that degradation efficiency was reduced from 93.25 to 86.63% for MB and 91.06 to 83.61 percent for Rh-B dyes, even after five cycles.

Also, FESEM was performed to check the morphology of ZnO NPs after the fifth cycle. Figure 16b shows that the FESEM outcome shows that ZnO NPs are slightly agglomerated, but the dye material still shows above 82% degradation for both. Besides, ZnO crystalline nature was analyzed in Fig. 16 using XRD analysis (c). The peak location was observed to remain the same with the decrease in peak intensity, which inferred that the ZnO photocatalysts crystal structure is not altered, even after several uses, the appreciable photostability of the ZnO photocatalyst.

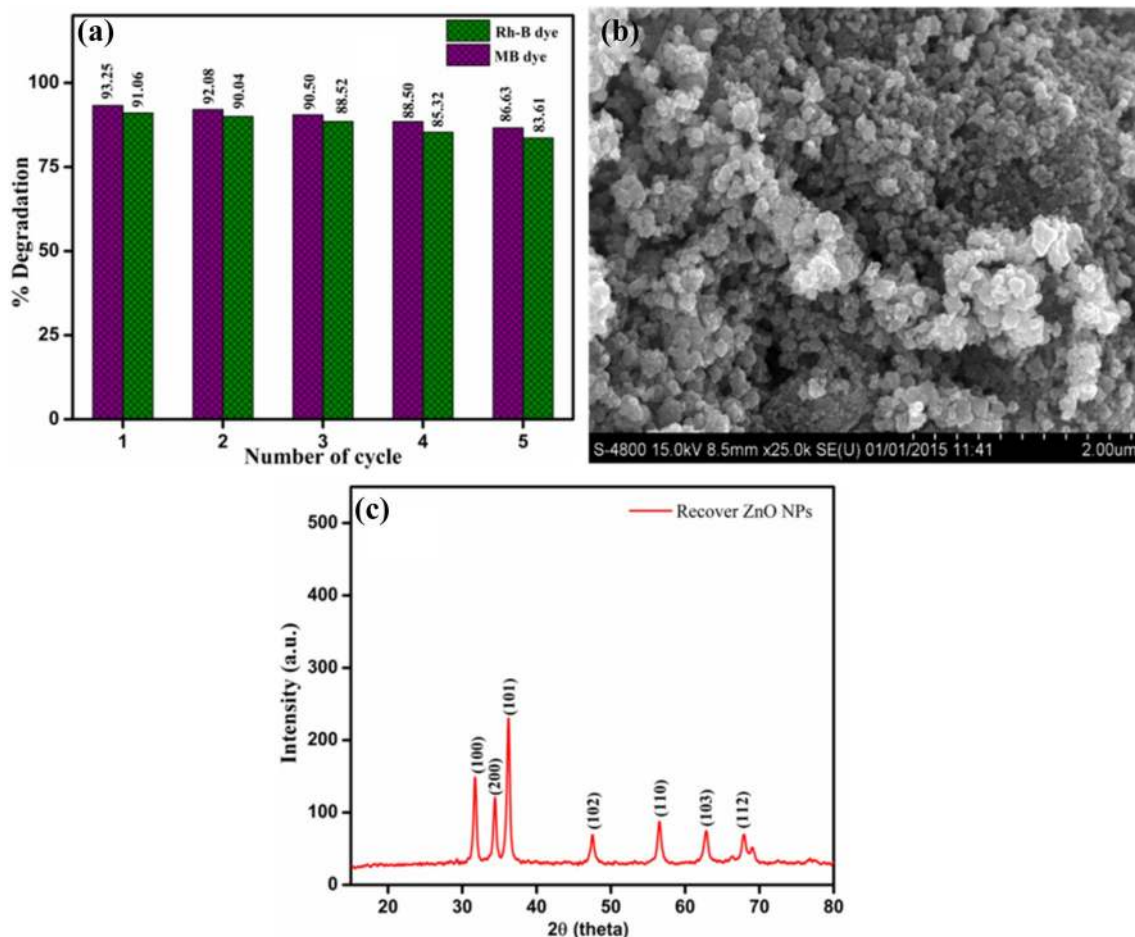


Fig. 16 **a** Reusability of ZnO photocatalyst, **b** FESEM and **c** XRD pattern of recovered ZnO

13 Conclusion

In the present study, ZnO NPs synthesis has been successfully synthesized using stinking passion Fruit peel extracts under a controlled ultrasound cavitation technique. The ZnO NPs were characterized in morphological, structural, and optical properties by FESEM, TEM, TGA, XRD, FTIR, and UV-DRS technique. The characterization of ZnO NPs revealed the formation of the polycrystalline wurtzite-structure of ZnO NPs. The morphology of ZnO NPs was found to be hexagonal and stone shape with a particle size of approximately 58 nm. Moreover, TGA explored ultrahigh thermal constancy of ZnO catalysts. ZnO is originated to be more stable (up to 410 °C) with 96.67% residue. The photocatalytic activity of ZnO NPs was investigated against MB and RhB dyes. The obtained result shows the 93.25% (MB) 0.0347 min^{-1} ($R^2 = 0.9026$) and 91.06% (Rh-B) 0.0337 min^{-1} ($R^2 = 0.9749$) dye within 70 min time period and degradation of dyes follow the pseudo-first-order kinetics. Further, ZnO NPs show excellent photocatalytic activity even after the 5th cycle and show good stability. This is because its

high stability and prodigious photocatalytic potential current study allude to green strategies-based photocatalyst and its effective wastewater treatment implementation.

Acknowledgements The author(s) disclosed receipt of the following financial support for the research, authorship, and publication of this article: The authors are thankful to UGC, New Delhi (UGC/MRP/43-157/2014(SR)) and DRDO, New Delhi (ERIP/ER/1503214/M/01/1745) for providing financial assistance to carry out this research work.

Declaration

Conflict of interest The authors have no conflict of interest.

Open Access This article is licensed under a Creative Commons Attribution 4.0 International License, which permits use, sharing, adaptation, distribution and reproduction in any medium or format, as long as you give appropriate credit to the original author(s) and the source, provide a link to the Creative Commons licence, and indicate if changes were made. The images or other third party material in this article are included in the article's Creative Commons licence, unless indicated otherwise in a credit line to the material. If material is not included in the article's Creative Commons licence and your intended use is not permitted by statutory regulation or exceeds the permitted

use, you will need to obtain permission directly from the copyright holder. To view a copy of this licence, visit <http://creativecommons.org/licenses/by/4.0/>.

References

1. Singh J, Dutta T, Kim KH, Rawat M, Samddar P, Kumar P (2018) "Green" synthesis of metals and their oxide nanoparticles: applications for environmental remediation. *J Nanobiotechnol* 16(1)
2. Singh J, Rathi A, Rawat M, Kumar V, Kim KH (2018) The effect of manganese doping on structural, optical, and photocatalytic activity of zinc oxide nanoparticles. *Compos B Eng*. <https://doi.org/10.1016/j.compositesb.2018.12.006>
3. Moradnia F, Taghavi F, Saeid R, Ali O, Samira A, Ilnaz (2020) Green sol-gel synthesis of CoMnCrO_4 spinel nanoparticles and their photocatalytic application. *Micro Nano Lett* 15(10):674–677
4. Taghavi F, Saeid R AO, Moradnia F, Afshari Z, Ganjkhanlu S, YekkeZare F (2019) Green synthesis of ZnO nanoparticles via Sol-gel method and investigation of its application in solvent-free synthesis of 12-Aryl-tetrahydrobenzo[a]xanthene-11-one derivatives under microwave irradiation. *Chem Methodol* 3(6):632–642
5. Shah AP, Jain S, Shimpi NG (2020) Enhanced photocatalytic activity of electrospun PAN/Ag-G NFs under solar irradiation for effective degradation of hazardous organic dyes. *ChemistrySelect* 5:3897–3905
6. Jain S, Shah AP, Shimpi NG (2020) An efficient photocatalytic degradation of organic dyes under visible light using zinc stannate (Zn_2SnO_4) nanorods prepared by microwave irradiation. *Nano-Struct Nano-Objects* 21:100410
7. Khan MS, Dhavan PP, Jadhav BL, Shimpi NG (2020) Ultrasound-assisted green synthesis of Ag-Decorated ZnO nanoparticles using *Excoecariaagalocha* leaf extract and evaluation of their photocatalytic and biological activity. *Chemistry Select* 5:2365–6549
8. Singh J, Kumar S, Alok A, Upadhyay SK, Rawat M DCW, Tsang BN, Ki-Hyun K (2019) The potential of green synthesized zinc oxide nanoparticles as nutrient source for plant growth. *J Clean Prod* 214:1061–1070
9. Taghavi FS, Moradnia F, Mostafaei M, Afshari Z, Faramarzi V, Ganjkhanlu S (2019) Biosynthesis of MgFe_2O_4 magnetic nanoparticles and its application in photodegradation of malachite green dye and kinetic study. *Nanochem Res* 4(1):86–93
10. Atrak K, Ramazani A, Taghavi F (2020) Green synthesis of $\text{Zn}_{0.5}\text{Ni}_{0.5}\text{AlFeO}_4$ magnetic nanoparticles and investigation of their photocatalytic activity for degradation of reactive blue 21 dye. *Environ Technol* 41(21):2760–2770
11. Wang J, Qiao M, Wei K, Ding J, Liu Z, Zhang K-Q, Huang X (2011) Decolorizing activity of Malachite Green and its mechanisms involved in dye biodegradation by *Achromobacterxylos oxidans* MG1. *J Mol Microbiol Biotechnol* 20:220–227
12. Ravelli D, Dondi D, Fagnoni M, Albin A (2009) Photocatalysis. A multi-faceted concept for green chemistry. *ChemSoc Rev* 38(7):1999
13. Yuvaraja S, Kumar V, Dhasmana H, Kumar A, Verma A, Jain VK (2019) Ultraviolet detection properties of electrodeposited n-SnO₂ modified p-Si nanowires hetero-junction photodiode. *J Mater Sci Mater Electron*. <https://doi.org/10.1007/s10854-019-01077-7>
14. Taghavi FS, Ramazani A, Woo Joo S (2017) Sol-gel synthesis and characterization of zinc oxide nanoparticles using Black Tea extract. *J Appl Chem Res* 11(4):8–17
15. Singh J, Kaur S, Kaur G, Basu S, Rawat M (2018) Biogenic ZnO nanoparticles: a study of blueshift of optical band gap and photocatalytic degradation of reactive yellow 186 dye under direct sunlight. *Green Process Synth*. <https://doi.org/10.1515/gps-2018-0084>
16. Mishra M, Chun DM (2015) $\alpha\text{-Fe}_2\text{O}_3$ as a photocatalytic material: a review. *ApplCatal A Gen* 498:126–141
17. Kaur G, Kaur H, Kumar S, Verma V, Jhinjer HS, Singh J, Al-Rashed S (2020) Blooming approach: one-pot biogenic synthesis of TiO_2 nanoparticles using piper betle for the degradation of Industrial Reactive Yellow 86 dye. *J InrgOrganometPolym Mater*. <https://doi.org/10.1007/s10904-020-01797-y>
18. Singh J, Kaur H, Rawat M (2018) A novel green approach for the synthesis of tungsten oxide nanorods and its efficient potential towards photocatalytic degradation of reactive green 19 dye. *J Mater Sci Mater Electron* 29(16):13715–13722
19. Ullah H, Mushtaq L, Ullah Z, Fazal A, Khan AM (2020) Effect of vegetable waste extract on microstructure, morphology, and photocatalytic efficiency of ZnO–CuO nanocomposites. *Inorg Nano-Met Chem*, pp 1–13
20. Jha M, Ansari S, Shimpi NG (2019) Ultrasonic assisted green synthesis of Ag: CdO nanocubes and nanospheres using Citrus limon leaves for efficient degradation of organic dyes. *J IndEngChem* 69:269–284
21. Su T, Shao Q, Qin Z, Guo Z, Wu Z (2018) Role of interfaces in two-dimensional photocatalyst for water splitting. *ACS Catal* 8:2253–2276
22. Khalid N, Majid A, Niaz TMB, Khalid NS (2017) Carbonaceous- TiO_2 nanomaterials for photocatalytic degradation of pollutants: a review. *Ceram Int* 43:14552–14571
23. Singh M, Singh J, Rawat M, Sharma J, Singh PP (2019) Enhanced photocatalytic degradation of hazardous industrial pollutants with inorganic–organic $\text{TiO}_2\text{-SnO}_2\text{-GO}$ hybrid nanocomposites. *J Mater Sci Mater Electro*. <https://doi.org/10.1007/s10854-019-01706>
24. Singh K, Singh J, Rawat M (2019) Green synthesis of zinc oxide nanoparticles using *Punica Granatum* leaf extract and its application towards photocatalytic degradation of Coomassie brilliant blue R-250 dye. *SN Appl Sci* 1(6). <https://doi.org/10.1007/s42452-019-0610-5>
25. Singh J, Kumar S, Alok A SK, Upadhyay MohitRawat, Tsang DCW, Bolan N, Kim KH (2019) The potential of green synthesized zinc oxide nanoparticles as nutrient source for plant growth. *J Clean Prod* 214:1061–1070
26. Prami N, Debajyoti D (2019) Photocatalytic degradation of Rhodamine-B dye by stable ZnO nanostructures with different calcination temperature induced defects. *Appl Surf Sci* 465:546–556
27. Alharthi FA, Alghamdi AA, Alothman AA, Almarhoon ZM, Alsulaiman MF, Al-Zaqri N (2020) Green synthesis of ZnO nanostructures using *salvadorapersica* leaf extract: applications for photocatalytic degradation of methylene blue dye. *Crystals* 10:441
28. Jha M, Shimpi NG (2018) Spherical nanosilver: bio-inspired green synthesis, characterizations, and catalytic applications. *Nano-Struct Nano-Objects* 16:234–249
29. Vinay SP, Chandrasekhar N (2020) Structural and Biological Investigation of Green Synthesized Silver and Zinc Oxide Nanoparticles. *J InorgOrganomet Polym Mater*, pp 1–7.
30. Singh J, Kumar V, Kim KH, Rawat M (2019) Biogenic synthesis of copper oxide nanoparticles using plant extract and its prodigious potential for photocatalytic degradation of dyes. *Environ Res*, 108569. <https://doi.org/10.1016/j.envres.2019.108569>
31. Lalitha K, Jong C, Ahn E, Jahan R, Suleman A, Jing L, Yang DC (2019) Synthesis of panos extract mediated ZnO nano-flowers as photocatalyst for industrial dye degradation by UV illumination. *J Photochem Photobiol* 199:111588
32. Ambasta SP (1986) The useful plants of India. Publication and Information Directorate, Council of Scientific and Industrial Research, India, New Delhi, pp 433–437

33. Chopra RL, Nayar SL, Chopra IC (1956) Glossary of Indian medicinal plants. Council of Scientific and Industrial Research, India, New Delhi, pp 186–187
34. Ezenwali MO, Njoku OU, Okoli CO (2009) Studies on the anti-diarrheal properties of seed extract of *Monodora tenuifolia*. *Int J App Res Nat Prod* 2:20–26
35. Lade BD, Patil AS (2017) Silver nano fabrication using leaf disc of *Passiflora foetida* Linn. *Appl Nanosci* 7:181–192
36. Renganathan S, Samar F, Kalainila P (2017) Green synthesis of copper nanoparticles from *para foetida* leaf extract and its antibacterial activity. *Asian J Pharm Clin Res* 10:79
37. Suganya D, Rajan MR, Ramesh R (2016) Green synthesis of iron oxide nanoparticles from leaf extract of *passiflora foetida* and its antibacterial activity. *Int J Curr Res* 8:42081–42085
38. Mittal AK, Chisti Y, Banerjee UC (2013) Synthesis of metallic nanoparticles using plant extracts. *Biotechnol Adv* 31:346–356
39. Rajaboopathi S, Thambidurai S (2018) Enhanced photocatalytic activity of Ag-ZnO nanoparticles synthesized by using *Padinagymnospora* seaweed extract. *J Mol Liq* 262:148–160
40. Moradnia F, Ramazani A, Fardood ST, Gouranlou F (2019) A novel green synthesis of and characterization of tetragonal-spinal MgMn₂₄ nanoparticles by tragacanth gel and studies of its photocatalytic activity for degradation of reactive blue 21 dye under visible light. *Mater Res Exp* 6:075057
41. Behzad EA, Ali RS, Ali M, (2008) Green synthesis and characterization of ZnAl₂O₄@ZnO nanocomposite and its environmental applications in rapid dye degradation. *Optik* 208:164129
42. Cinteza LO, Scamoroscenco C, Voicu SN, Nistor CL, Nitu SG, Trica B, Jecu M, Petcu C (2018) Chitosan-stabilized Ag nanoparticles with superior biocompatibility and their synergistic antibacterial effect in mixtures with essential oils. *J Nanomat* 8:1–16
43. Yeon JS, Veronika S, Gokulanathan A, Ramya M (2019) Zinc oxide nanoparticles synthesized by *Suaeda japonica* Makino and their photocatalytic degradation of methylene blue. *Optik* 182:1015–1020
44. Kavita S, Sini K, Jaspal S, Biswarup S, Satyabrata M (2018) Facile synthesis of ZnO nanoplates and nanoparticle aggregates for highly efficient photocatalytic degradation of organic dyes. *J Phys Chem Solids* 121:86–195
45. Chandran SP, Chaudhary M, Pasricha R, Ahmad A, Sastry M (2006) Synthesis of gold nanotriangles and silver nanoparticles using *Aloe vera* plant extract. *Biotechnol Prog* 22:577–583
46. Jia L, Zhang Q, Li Q, Song H (2009) The biosynthesis of palladium nanoparticles by antioxidants in *Gardenia jasminoides* Ellis: Long lifetime nanocatalysts for p-nitrotoluene hydrogenation. *J Nanotechnol* 20:385601
47. Vishnukumar P, Vivekanandhan S, Misra M, Mohanty AK (2018) Recent advances and emerging opportunities in phytochemical synthesis of ZnO nanostructures. *Mater Sci Semicond Process* 80:143–161
48. Madan H, Sharma S, Suresh D, Vidya Y, Nagabhushana H, Rajanaik H, Anautharaju KS, Prashantha SC, SadanandaMaiya P (2016) Facile green fabrication of nanostructure ZnO plates, bullets, flower, prismatic tip, closed pine cone: their antibacterial, antioxidant, photoluminescent and photocatalytic properties. *Spectrochim Acta Mol Biomol Spectrosc* 152:404–416
49. Moradnia F, STF, Ali R, Gupta VK (2020) Green synthesis of recyclable MgFeCrO₄ spinel nanoparticles for rapid photodegradation of direct black 122 dye. *J Photochem Photobiol A Chem* 392:112433
50. Ahankar H, Fardood ST, Ramazani (2020) One-pot three component synthesis of tetrahydrobenzo[b]pyrans in the presence of Ni_{0.5}Fe_{2.0}O₄ magnetic nanoparticles under microwave irradiation in solvent free conditions. *Iran JCatal* 10:195–201
51. Taghavi FS, Moradnia F, Ghalaichi A, Danesh P, Heidari M (2020) Facile green synthesis and characterization of zinc oxide nanoparticles using tragacanth gel: investigation of their photocatalytic performance for dye degradation under visible light irradiation. *Nanochem Res* 5(1):69–76
52. Dizavandi ZR, Aliakbar A, Sheykhani M (2017) Electrochemical determination of clopidogrel using Bi₂O₃-Pp-AP/GCE by differential pulse voltammetry in pharmaceutical productions. *J Electroanal Chem* 805:24–31
53. Rao NS, Rao MVB (2015) Structural and optical investigation of ZnO nanopowders synthesized from Zinc Chloride and Zinc Nitrate. *Am J Mater Sci* 5:66–68
54. Taghavi FS, Moradnia F RA (2019) Green synthesis and characterization of ZnMn₂O₄ nanoparticles for photocatalytic degradation of Congo red dye and kinetic study. *Micro Nano Lett* 14(9):986–991
55. Shah AP, Shilpa J, Mokale VJ, Shimpi NG (2019) High performance visible light photocatalysis of electrospun PAN/ZnO hybrid nanofibers. *J Indus Eng Chem* 77:154–163
56. JhaMinakshi AS, Shimpi NG (2019) Ultrasonic assisted green synthesis of Ag: CdO nanocubes and nanospheres using *Citrus limon* leaves for efficient degradation of organic dyes. *J Indust Eng Chem* 69:269–284
57. Kavita S, Sini K, Jaspal S, Biswarup S, Mohapatra S (2018) Facile synthesis of ZnO nanoplates and nanoparticle aggregates for highly efficient photocatalytic degradation of organic dyes. *J Phys Chem Solids* 121:186–195
58. Rani P, Kumar V, Singh PP, Matharu AS, Zhang W, Kim KH, Rawat M (2020) Highly stable AgNPs prepared via a novel green approach for catalytic and photocatalytic removal of biological and non-biological pollutants. *Environ Inter* 143:105924
59. Mohammed R, Ali MEM, Gomaa E, Mohsen M (2020) Green ZnO nanorod material for dye degradation and detoxification of pharmaceutical wastes in water. *J Environ Chem Eng*, 104295
60. Bansal P, Sud D (2012) Photodegradation of commercial dye, CI Reactive Blue 160 using ZnO nanopowder: degradation pathway and identification of intermediates by GC/MS. *Sep Purif Technol.* <https://doi.org/10.1016/j.seppur.2011.09.055>
61. Kaur N, Singh J, Kumar S, Singh P, Al-Rashed S, Kaur H, Rawat M (2020) An efficient and viable photodegradation of a textile Reactive yellow-86 dye under direct sunlight by multi-structured Fe₂O₃ encapsulated with phytochemicals of *R. Indica*. *J Mater Sci Mater Electron*
62. Zhang X, Zhang S, Dong X, Zhou S, Dong (2016) N-doped carbon quantum dots/TiO₂ hybrid composites with enhanced visible light driven photocatalytic activity toward dye wastewater degradation and mechanism insight. *J Photochem Photobiol A Chem* 325:104–110
63. Ming H, Ma Z, Liu Y, Pan K, Yu H, Wang F, Kang Z (2012) Large scale electrochemical synthesis of high quality carbon nanodots and their photocatalytic property. *Dalton Trans* 41:9526–9531
64. Yu BY, Kwak SY (2012) Carbon quantum dots embedded with mesoporous hematite nanospheres as efficient visible light-active photocatalysts. *J Mater Chem* 22:8345–8353
65. Bozetine H, Wang Q, Barras A, Li M, Hadjersi T SS, Boukherroub R (2016) Green chemistry approach for the synthesis of ZnO-carbon dots nanocomposites with good photocatalytic properties under visible light. *J Colloid Interface Sci* 465:286–294
66. Song B, Wang T, Sun H, Shao Q, Zhao J, Song K, Hao L WL, Guo Z (2017) Twostep hydrothermally synthesized carbon nanodots/WO₃ photocatalysts with enhanced photocatalytic performance. *Dalton Trans* 46:15769–15777
67. Serrà A, Zhang Y, Sepúlveda B, Gómez E, Nogués J, Michler J, Philippe L (2019) Highly active ZnO-based biomimetic fern-like microleaves for photocatalytic water decontamination using sunlight. *Appl Catal B Environ.* <https://doi.org/10.1016/j.apcatb.2019.02.017>

68. Isai KA, Shrivastava VS (2019) Photocatalytic degradation of methylene blue using ZnO and 2%Fe–ZnO semiconductor nanomaterials synthesized by sol–gel method: a comparative study. *SN Appl Sci* 1:1247
69. Tian L, Rui Y, Sun K, Cui W, An W (2018) Surface decoration of ZnWO₄ Nanorods with Cu₂O nanoparticles to build heterostructure with enhanced photocatalysis. *Nanomaterials* 8(1):33
70. Suresh M, Sivasamy A (2018) Bismuth oxide nanoparticles decorated Graphene layers for the degradation of Methylene blue dye under visible light irradiations and antimicrobial activities. *J Environ Chem Eng* 6(3):3745–3756
71. AminiM AM (2016) Photocatalytic degradation of some organic dyes under solar light irradiation using TiO₂ and ZnO nanoparticles. *Nanochem Res* 1:79–86
72. Huerta-Flores AM, Sánchez-Martínez D, delRocío H-R, Zarazúa-Morín ME, Torres-Martínez LM (2018) Visible-light-driven BaBiO₃ perovskite photocatalysts: effect of physicochemical properties on the photoactivity towards water splitting and the removal of rhodamine B from aqueous systems. *J Photochem Photobiol A Chem*. <https://doi.org/10.1016/j.jphotochem.2018.09.025>
73. Tavakoli-Azar T, Reza Mahjoub A, SeyedSadjadi M, Farhadyar N, Hossaini Sadr M (2020) Improving the photocatalytic performance of a perovskite ZnTiO₃ through ZnTiO₃@S nanocomposites for degradation of Crystal violet and Rhodamine B pollutants under sunlight. *Inorg Chem Commun* 119:108091

Publisher's Note Springer Nature remains neutral with regard to jurisdictional claims in published maps and institutional affiliations.